JGR Space Physics

METHOD

10.1029/2024JA033584

An Efficient Positivity-Preserving Finite Difference Scheme for Solving the Fokker-Planck Diffusion Equation

Chengjie Qi[1,2,3], **Zhenpeng Su**[1,2,3,4], **Zhiyong Wu**[1,2,3], **Huinan Zheng**[1,2,3], and **Yuming Wang**[1,2,3]

[1]National Key Laboratory of Deep Space Exploration/School of Earth and Space Sciences, University of Science and Technology of China, Hefei, China, [2]CAS Center for Excellence in Comparative Planetology/CAS Key Laboratory of Geospace Environment/Mengcheng National Geophysical Observatory, University of Science and Technology of China, Hefei, China, [3]Collaborative Innovation Center of Astronautical Science and Technology, Harbin, China, [4]State Key Laboratory of Lunar and Planetary Sciences, Macau University of Science and Technology, Macao, China

Key Points:

- The semi-implicit logarithmic linearization finite difference scheme is developed for solving the Fokker-Planck diffusion equation
- The basic principle is to linearize the nonlinear equation of the natural logarithmic phase space density
- This scheme balances positivity preservation, efficiency, and simplicity but exhibits oversensitivity to near vanishing phase space densities

Correspondence to:

Z. Su,
szpe@mail.ustc.edu.cn

Citation:

Qi, C., Su, Z., Wu, Z., Zheng, H., & Wang, Y. (2025). An efficient positivity-preserving finite difference scheme for solving the Fokker-Planck diffusion equation. *Journal of Geophysical Research: Space Physics*, *130*, e2024JA033584. https://doi.org/10.1029/2024JA033584

Received 27 NOV 2024
Accepted 2 APR 2025

Abstract The Fokker-Planck diffusion equation is widely used for simulating the evolution of Earth's radiation belt electrons, which pose significant hazards to space-borne systems. To preserve the positivity of the numerical solution of the electron phase space density (PSD), several finely designed finite difference, Monte Carlo, spatiotemporal interpolation, and finite volume schemes have been developed. However, these schemes often suffer from either high implementation complexity or low execution efficiency. Here we propose an efficient, easy-to-implement, and positivity-preserving finite difference scheme, named the Semi-Implicit Logarithmic Linearization (SILL) scheme. The basic principle is to linearize the nonlinear equation of the natural logarithmic PSD. This scheme ensures accuracy and stability, even with large time steps, up to hundreds of seconds for typical radiation belt electron diffusion processes. Nonetheless, it exhibits oversensitivity to near-vanishing phase space densities, which necessitates reduced time steps when handling extremely large variations in orders of magnitude between neighboring grid points. We have publicly released the protype code of the SILL scheme, which could be useful for the radiation belt modeling community.

1. Introduction

Earth's radiation belt electrons exhibit dramatic dynamics (e.g., Blake et al., 1992; Baker et al., 2004; Horne, Thorne, Shprits, et al., 2005; X. Li et al., 2001; W. Li & Hudson, 2019; Miyoshi et al., 2004; Reeves et al., 2003; Reeves et al., 2013; Ripoll et al., 2020; Zong et al., 2009) and pose significant hazards to space-borne systems (e.g., Horne et al., 2013). Wave-particle interactions are commonly regarded as one of the primary mechanisms for the evolution of radiation belt electrons (Thorne, 2010). To understand and forecast the wave-driven evolution of global radiation belt electrons, quasi-linear Fokker-Planck diffusion models have been widely adopted (Schulz & Lanzerotti, 1974; Lyons & Williams, 1984; Beutier & Boscher, 1995; Summers et al., 1998; Horne & Thorne, 1998; W. Li et al., 2007; Varotsou et al., 2008; Summers et al., 2007a, 2007b; Fok et al., 2008; Albert et al., 2009; Xiao et al., 2009, 2010; Su, Xiao, et al., 2010; Su et al., 2011a; Bortnik & Thorne, 2010; J. Li et al., 2014; L. Y. Li et al., 2017; Ni et al., 2019; Zhao et al., 2019;, Shprits, 2009; D. A. Subbotin & Shprits, 2009, 2012; Tu et al., 2013; Shprits et al., 2013; Thorne et al., 2013; Glauert et al., 2014; Xiao et al., 2015; He et al., 2016; C. Wang et al., 2017; Yuan et al., 2018; Fu et al., 2019; D. Wang et al., 2020; Yu et al., 2024, and others). The Fokker-Planck diffusion equation describes the evolution of electron PSD, and the positivity of the numerical solution is a fundamental physical requirement. However, the presence of cross-diffusion terms has proven to pose a significant challenge in preserving the positivity of the numerical solutions (Albert, 2013; Camporeale et al., 2013a, 2013b, 2013c).

Until now, three classes of positivity-preserving techniques have been proposed to solve the Fokker-Planck diffusion equation. The first class involves applying the traditional Fully Implicit (FI) finite difference scheme to the diffusion equation after diagonalizing it through coordinate transformation (Albert, 2018; Albert & Young, 2005). The second class involves utilizing Monte Carlo methods or spatiotemporal interpolation methods to a set of stochastic differential equations reformulated from the original diffusion equation (Tao et al., 2008, 2016). The third class involves introducing a nonlinear two-point flux approximation in the finite volume scheme to solve the diffusion equation (Gao & Wu, 2015; Peng et al., 2024). However, compared to other finite difference techniques (Xiao et al., 2009; D. Subbotin et al., 2010; Camporeale et al., 2013a, 2013b, 2013c), which may not

preserve the positivity of the numerical solutions (Albert, 2013), these positivity-preserving techniques often suffer from either higher implementation complexity or lower execution efficiency.

In this study, we propose a new positivity-preserving finite difference scheme, named Semi-Implicit Logarithmic Linearization (SILL) scheme, for solving the Fokker-Planck diffusion equation. Our tests demonstrate that this novel scheme balances positivity preservation, ease of implementation, efficiency, and accuracy.

2. Construction of SILL Scheme

The Fokker-Planck diffusion equation for the evolution of the PSD f in a general coordinate system $\sigma = (\sigma_1, \sigma_2, \sigma_3)$ can be written as (Schulz & Lanzerotti, 1974)

$$\frac{\partial f}{\partial t} = \sum_{i=1}^{3}\sum_{j=1}^{3}\frac{1}{G}\frac{\partial}{\partial \sigma_i}\left(GD_{\sigma_i\sigma_j}\frac{\partial f}{\partial \sigma_j}\right), \tag{1}$$

with the time t, the Jacobian transformation parameter G, and the diffusion matrix $D_{\sigma_i\sigma_j}$. Achieving numerical stability in solving this equation requires $D_{\sigma_i\sigma_i}D_{\sigma_j\sigma_j} > D^2_{\sigma_i\sigma_j}$ when $i \neq j$ (Albert, 2004; Gourlay & McKee, 1977; Richtmyer & Morton, 1967). Applying a natural logarithmic transformation

$$h = \ln\frac{f}{\max\left(f|_{t=0}\right)} \tag{2}$$

is a straightforward approach to ensure the positivity of $f = \max\left(f|_{t=0}\right)\exp(h)$. However, this transformation introduces nonlinearity into the equation for h

$$\frac{\partial h}{\partial t} = \sum_{i,j}\frac{1}{G}\left(\frac{\partial (GD_{\sigma_i\sigma_j})}{\partial \sigma_i}\frac{\partial h}{\partial \sigma_j} + GD_{\sigma_i\sigma_j}\frac{\partial^2 h}{\partial \sigma_i \partial \sigma_j} + GD_{\sigma_i\sigma_j}\frac{\partial h}{\partial \sigma_i}\frac{\partial h}{\partial \sigma_j}\right). \tag{3}$$

With the operator splitting technique (Kim et al., 1999; Strang, 1968), the multi-dimensional problem is divided into three sub-problems

$$\begin{aligned}\frac{\partial h}{\partial t} = {} & D_{\sigma_i\sigma_i}\frac{\partial^2 h}{\partial \sigma_i^2} + \left(\sum_{j=1}^{3}\frac{1}{G}\frac{\partial (GD_{\sigma_i\sigma_j})}{\partial \sigma_j}\right)\frac{\partial h}{\partial \sigma_i} + D_{\sigma_i\sigma_i}\left(\frac{\partial h}{\partial \sigma_i}\right)^2 \\ & + \sum_{j}^{i\neq j}\left[D_{\sigma_i\sigma_j}\frac{\partial^2 h}{\partial \sigma_i \partial \sigma_j} + D_{\sigma_i\sigma_j}\frac{\partial h}{\partial \sigma_i}\frac{\partial h}{\partial \sigma_j}\right], \\ & i = 1,\ 2,\ \text{and}\ 3.\end{aligned} \tag{4}$$

At each time step, the solution process starts with the sub-problem for $i = 1$, proceeds to the sub-problem for $i = 2$ using the solution from the first as an initial condition, and then concludes with the sub-problem for $i = 3$, utilizing the solution from the immediately preceding step. Given that the sub-problems listed in Equation 4 are not solved in isolation over an extended period, a detailed theoretical analysis of the numerical behavior of any individual sub-problem may not be appropriate in this context. Equation 4 may be written in a more general form

$$\frac{\partial w}{\partial t} = a\frac{\partial^2 w}{\partial x^2} + b\frac{\partial w}{\partial x} + c\left(\frac{\partial w}{\partial x}\right)^2 + d(w), \tag{5}$$

which is discretized with a time step Δt and a spatial grid size Δx in the finite difference framework. A semi-implicit scheme (Strang, 1968) is expressed as

$$\frac{w_i^{n+1} - w_i^n}{\Delta t} = a_i\left[\frac{\partial^2 w}{\partial x^2}\right]_i^{n+1} + b_i\left[\frac{\partial w}{\partial x}\right]_i^{n+1} + c_i\left[\left(\frac{\partial w}{\partial x}\right)^2\right]_i^{n+1/2} + [d(w)]_i^n, \tag{6}$$

where the superscript n represents the nth time step, the superscript $1/2$ presents half a time step, and the subscript i represents the ith spatial grid. The nonlinear term can be linearized using a geometric mean (Evans & Sanugi, 1987)

$$\left[\left(\frac{\partial w}{\partial x}\right)^2\right]_i^{n+1/2} \sim \left[\frac{\partial w}{\partial x}\right]_i^n \left[\frac{\partial w}{\partial x}\right]_i^{n+1}. \tag{7}$$

The geometric mean exhibits the same second-order temporal accuracy as the commonly used arithmetic mean, a property that can be readily verified through Taylor expansion

$$\left[\frac{\partial w}{\partial x}\right]_i^n = \left[\frac{\partial w}{\partial x}\right]_i^{n+\frac{1}{2}} - \frac{\Delta t}{2}\left[\frac{\partial^2 w}{\partial x^2}\right]_i^{n+\frac{1}{2}} + O(\Delta t^2), \tag{8}$$

$$\left[\frac{\partial w}{\partial x}\right]_i^{n+1} = \left[\frac{\partial w}{\partial x}\right]_i^{n+\frac{1}{2}} + \frac{\Delta t}{2}\left[\frac{\partial^2 w}{\partial x^2}\right]_i^{n+\frac{1}{2}} + O(\Delta t^2), \tag{9}$$

$$\left[\frac{\partial w}{\partial x}\right]_i^n \left[\frac{\partial w}{\partial x}\right]_i^{n+1} = \left[\left(\frac{\partial w}{\partial x}\right)^2\right]_i^{n+1/2} + O(\Delta t^2). \tag{10}$$

Then Equation 6 becomes

$$\frac{w_i^{n+1} - w_i^n}{\Delta t} = a_i\left[\frac{\partial^2 w}{\partial x^2}\right]_i^{n+1} + \overline{b}_i^n\left[\frac{\partial w}{\partial x}\right]_i^{n+1} + [d(w)]_i^n, \tag{11}$$

with

$$\overline{b}_i^n = b_i + c_i\left[\frac{\partial w}{\partial x}\right]_i^n. \tag{12}$$

On the right-hand side of Equation 11, the second-order implicit central difference is used for the first diffusion term

$$\left[\frac{\partial^2 w}{\partial x^2}\right]_i^{n+1} \sim \frac{w_{i+1}^{n+1} - 2w_i^{n+1} + w_{i-1}^{n+1}}{\Delta x^2}; \tag{13}$$

the first-order implicit upwind difference is used for the second advection term

$$\left[\frac{\partial w}{\partial x}\right]_i^{n+1} \sim -\mathrm{sign}\left(\overline{b}_i^n\right)\frac{w_i^{n+1} - w_{i+\mathrm{sign}\left(\overline{b}_i^n\right)}^{n+1}}{\Delta x}, \tag{14}$$

which is critical to make the solver stable by introducing sufficient numerical dissipation; the second-order explicit central differences are used for the all the spatial derivatives of diffusion coefficients and w in $\overline{b}_i^n$ and $[d(w)]_i^n$. The discretization above leads to a tridiagonal system of linear equations that is computationally inexpensive to solve. This numerical scheme is referred to as the SILL scheme, reflecting its distinctive characteristics.

Due to the difference in operator splitting, the SILL scheme requires solving a tridiagonal system of linear equations only half as many times as the previously developed Hybrid Finite Difference (HFD) scheme (Xiao et al., 2009). However, compared to the HFD and other schemes that do not employ the natural logarithmic transformation, the SILL scheme shows oversensitivity to near-vanishing PSDs. For example, while the spatial variation of PSDs from $f = 10^{-2}$ to 10^{-1} is significant, the spatial variation of PSDs from $f = 10^{-200}$ to 10^{-100} is

negligible. When applying the natural logarithmic transformation, the transformed PSD exhibits a much larger spatial gradient for the latter case compared to the former case. This increased sensitivity imposes additional constraints on time step, necessitating smaller time steps to prevent numerical instability and accurately capture the PSD behavior. An extreme situation arises when $f = 0$, where the direct application of the natural logarithmic transformation is undefined, requiring special treatments in the SILL scheme to handle such cases.

3. Numerical Tests

3.1. Simplified One-Dimensional Diffusion Tests

An one-dimensional diffusion equation is written as

$$\frac{\partial f}{\partial t} = D\frac{\partial^2 f}{\partial x^2}, \tag{15}$$

where the diffusion coefficient $D = 1$. The initial condition is designed as

$$f = \frac{1}{p^2} e^{-\left(\frac{E-1}{0.2}\right)^2}, \tag{16}$$

$$p = e^x, \tag{17}$$

$$E = 0.511\left(\sqrt{1+p^2} - 1\right), \tag{18}$$

in the computational domain $E \in [0.2, 5.0]$. The boundary conditions are specified as

$$\left.\frac{\partial f}{\partial x}\right|_{E=0.2} = 0, \tag{19}$$

$$\left.\frac{\partial f}{\partial x}\right|_{E=5.0} = 0. \tag{20}$$

Figure 1 shows the simulation results from the SILL scheme and the FI scheme. The computational domain is discretized into 50 uniformly spaced grids along x. We first focus on the results obtained using a time step of $\Delta t = 10^{-4}$. Both schemes produce positive PSDs from $t = 0$ to $t = 0.1$, and over longer time scales, such as $t = 0.1$, they yield generally consistent results. However, compared to the FI scheme, the SILL scheme is more capable of capturing extremely subtle changes in PSDs at higher energies ($E > 2$). For example, at $E = 5.0$ within the first time step, f increases from 1.7×10^{-176} to 2.5×10^{-126} in the SILL results but increases from 1.7×10^{-176} to 1.3×10^{-32} in the FI results. If one does not care about such subtle variations in PSDs, the extreme accuracy of the SILL scheme can become an oversensitivity limitation. When the time step in the SILL scheme is sufficiently large, for example, $\Delta t = 0.1$, the results can become distorted. In contrast, the results from the FI scheme are less sensitive to the time step.

3.2. Simplified Two-Dimensional Diffusion Tests

A simple two-dimensional diffusion equation introduced by Albert (2013) is

$$\frac{\partial f}{\partial t} = \frac{\partial}{\partial x}\left[D_{xx}\frac{\partial f}{\partial x} + D_{xy}\frac{\partial f}{\partial y}\right] + \frac{\partial}{\partial y}\left[D_{xy}\frac{\partial f}{\partial x} + D_{yy}\frac{\partial f}{\partial y}\right], \tag{21}$$

with the diffusion coefficients $D_{xx} = 1$, $D_{yy} = 1$, and $D_{xy} = 0.8$, the computational domain $x \in [0, 1]$ and $y \in [0, 1]$, the initial condition

$$f|_{t=0} = e^{-y/0.02}\sin(\pi x/2), \tag{22}$$

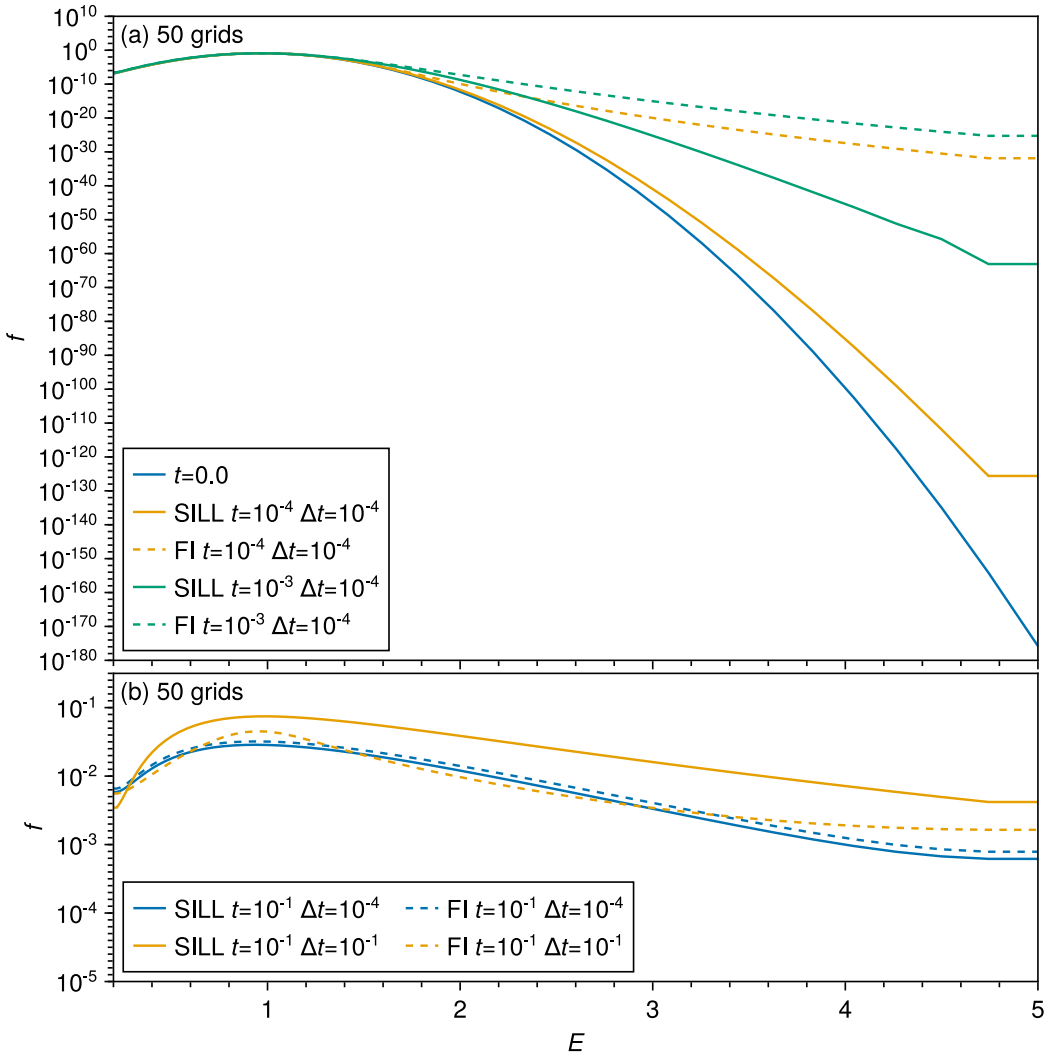

Figure 1. Comparison between numerical solutions of the simplified one-dimensional diffusion problem with the Semi-Implicit Logarithmic Linearization (solid lines) and Fully Implicit (dashed lines) schemes.

and the boundary conditions

$$f|_{x=0} = 0,\ \left.\frac{\partial f}{\partial x}\right|_{x=1} = 0,\ f|_{y=0} = f|_{t=0,\ y=0},\ \left.\frac{\partial f}{\partial y}\right|_{y=1} = 0. \tag{23}$$

To avoid taking the logarithm of zero values in the SILL scheme, the left boundary is artificially moved from $x = 0$ to $x = \Delta x$ and the correspoing boundary condition is implemented as

$$f|_{x=\Delta x,t} = \frac{1}{2} f|_{x=2\Delta x,t}. \tag{24}$$

This boundary condition can be interpreted as an approximation of $f|_{x=\Delta x}$ using central interpolation

$$f|_{x=\Delta x,t} = \frac{f|_{x=0,t} + f|_{x=2\Delta x,t}}{2}, \tag{25}$$

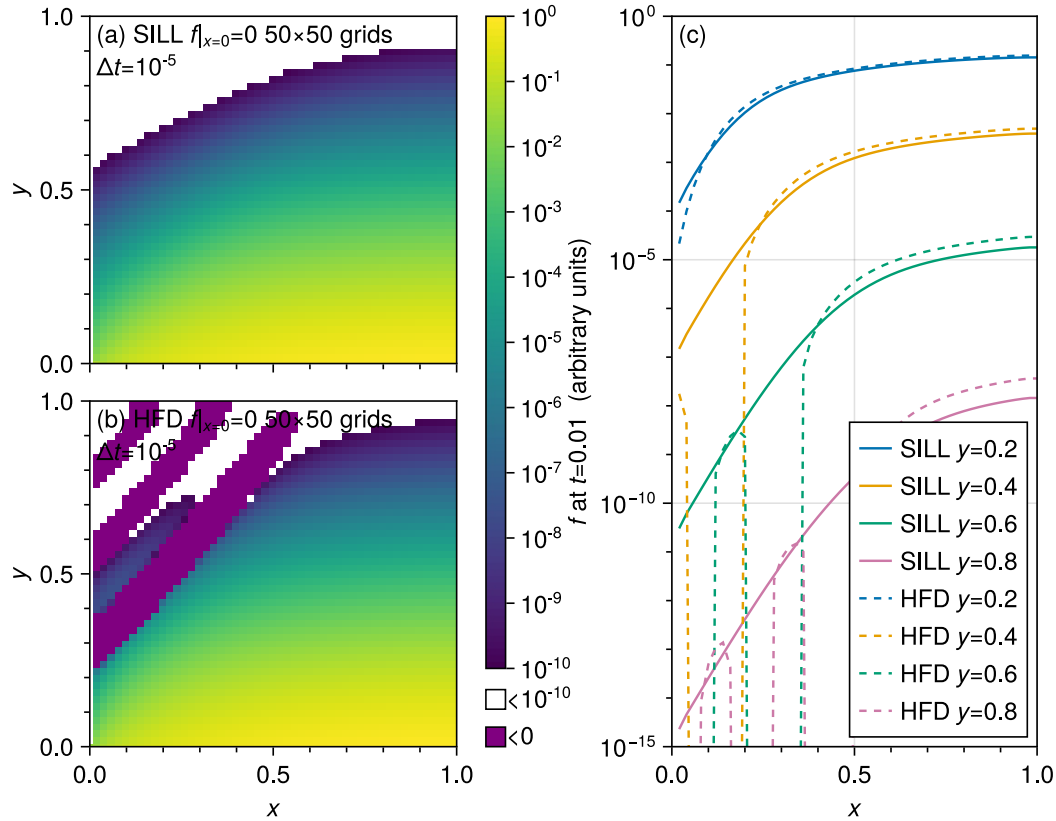

Figure 2. Numerical solutions of the simplified two-dimensional diffusion problem at $t = 0.01$. Two-dimensional PSDs (color-coded) from the (a) Semi-Implicit Logarithmic Linearization (SILL) and (b) Hybrid Finite Difference (HFD) schemes in the x–y plane. (c) Comparison between phase space density profiles from SILL (sold lines) and HFD (dashed lines) schemes. Colors help differentiate among the x-dependent profiles at different y values.

where

$$f|_{x=0,t} = 0. \tag{26}$$

After the natural logarithmic transformation $h = \ln f$, this implicit boundary condition becomes

$$h|_{x=\Delta x,t} = h|_{x=2\Delta x,t} - \ln 2, \tag{27}$$

which can be directly included in the tridiagonal system of linear equations.

Figure 2 presents the simulation results from the SILL and HFD schemes at $t = 0.01$. The computational domain is evenly divided into 50×50 grids, and the time step is set to be $\Delta t = 10^{-5}$. The SILL scheme gives a smooth, positivity-preserving solution throughout the computational domain. In contrast, a series of negative stripes extending from the left boundary to the upper boundary arise in the HFD solution, similar to the results given by Albert (2013). Apart from those nonphysical negative PSD values, the HFD solution is generally consistent with the SILL solution. Near the right boundary, unlike the solution given by the positivity-preserving finite volume scheme (Figure 3 of Peng et al., 2024), which shows an abnormal upward increase in PSD values, both the HFD and SILL solutions yield flat PSD profiles, which appear to be more compatible with the right boundary condition.

3.3. Realistic Two-Dimensional Diffusion Tests

The evolution of electron PSD driven by plasma waves through violating the first and second adiabatic invariants in the space of pitch-angle α and momentum p can be written as (e.g., Albert, 2004; Lyons & Williams, 1984)

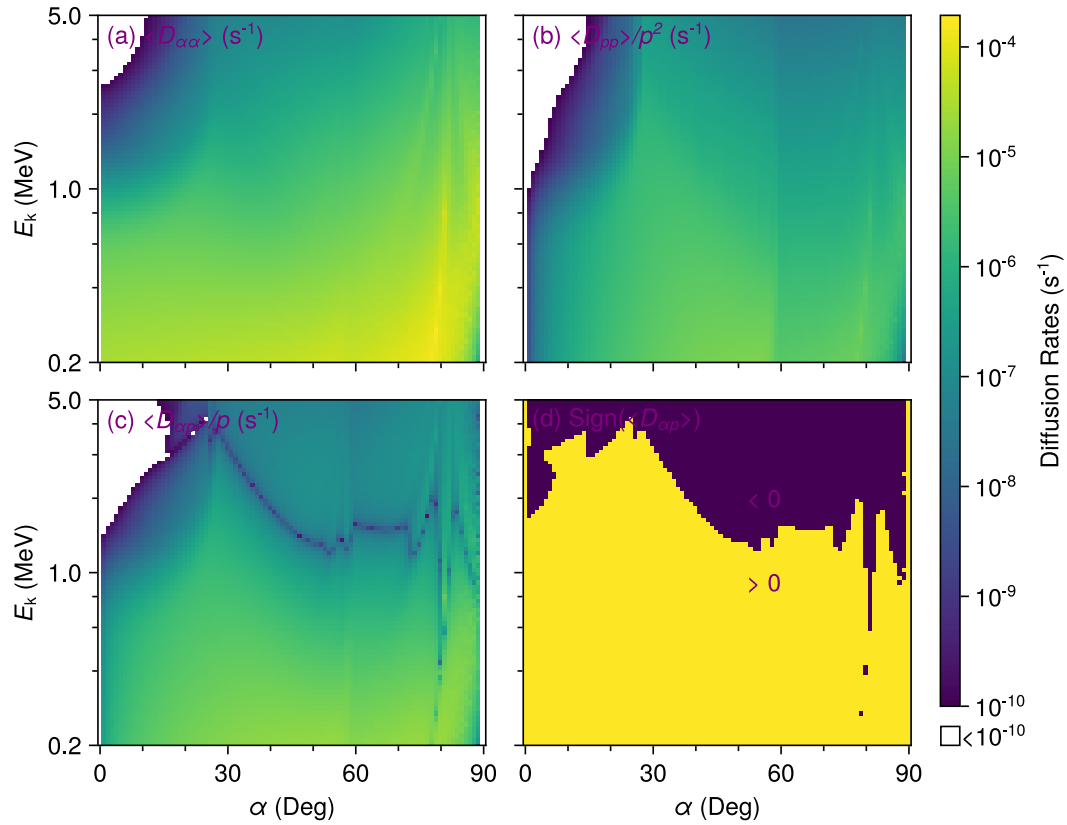

Figure 3. Diffusion rates of chorus waves. (a) Pitch-angle diffusion rate $\langle D_{\alpha\alpha}\rangle$. (b) Momentum diffusion rate $\langle D_{pp}\rangle/p^2$. (c) Cross diffusion rate $\langle D_{\alpha p}\rangle/p$. (d) Sign of cross diffusion rate Sign($\langle D_{\alpha p}\rangle$).

$$\frac{\partial f}{\partial t} = \frac{1}{G}\frac{\partial}{\partial \alpha}\left[G\left(\langle D_{\alpha\alpha}\rangle\frac{\partial f}{\partial \alpha} + \langle D_{\alpha p}\rangle\frac{\partial f}{\partial p}\right)\right] + \frac{1}{G}\frac{\partial}{\partial p}\left[G\left(\langle D_{p\alpha}\rangle\frac{\partial f}{\partial \alpha} + \langle D_{pp}\rangle\frac{\partial f}{\partial p}\right)\right] - \frac{f}{\tau_L}, \tag{28}$$

where $G = p^2(1.30 - 0.56\sin\alpha)\sin\alpha\cos\alpha$ is the Jacobian transformation parameter, and $\langle D_{\alpha\alpha}\rangle$, $\langle D_{\alpha p}\rangle = \langle D_{p\alpha}\rangle$, and $\langle D_{pp}\rangle$ represent the pitch angle, cross, and momentum diffusion coefficients, respectively, and the term $-f/\tau_L$ characterizes the precipitation loss within the bounce loss cone (Shprits et al., 2009). To better capture the electron energy spectrum, a simple variable transformation (Xiao et al., 2009) is applied to Equation 28

$$\xi = \ln\frac{p}{m_e c} \tag{29}$$

with the electron mass m_e and the speed of light c. Then Equation 28 becomes

$$\frac{\partial f}{\partial t} = \frac{1}{G}\frac{\partial}{\partial \alpha}\left[G\left(\langle D_{\alpha\alpha}\rangle\frac{\partial f}{\partial \alpha} + \frac{\langle D_{\alpha p}\rangle}{p}\frac{\partial f}{\partial \xi}\right)\right] + \frac{1}{Gp}\frac{\partial}{\partial \xi}\left[G\left(\langle D_{p\alpha}\rangle\frac{\partial f}{\partial \alpha} + \frac{\langle D_{pp}\rangle}{p}\frac{\partial f}{\partial \xi}\right)\right] - \frac{f}{\tau_L}. \tag{30}$$

There have been two types of boundary treatments near the bounce loss cone. One treatment is to set τ_L to be 1/4 bounce period in the loss cone $\alpha < \alpha_L$ and infinite outside the loss cone, and introduce the equivalent extrapolation boundary condition $\partial f/\partial\alpha = 0$ at the left pitch-angle boundary $\alpha = 0°$ (Shprits et al., 2009). The other treatment is to set the fixed boundary condition $f|_{\alpha=\alpha_L} = 0$ at the left pitch-angle boundary $\alpha = \alpha_L$, equivalent to setting $\tau_L = 0$ in the loss cone $\alpha < \alpha_L$ (e.g., Selesnick et al., 2003; Albert & Young, 2005; W. Li et al., 2007; Tu

et al., 2010; Pham et al., 2017). The former treatment is applicable for both the strong and weak diffusion problems, while the latter treatment is applicable only for the weak diffusion problems (Shprits et al., 2009; Su et al., 2011b; Su, Zheng, & Wang, 2010). At the right pitch-angle boundary $\alpha = 90°$, the equivalent extrapolation boundary condition $\partial f/\partial\alpha = 0$. The computational domain of electron kinetic energy E_k is [0.2 MeV, 5.0 MeV], with the fixed boundary condition at $E_k = 0.2$ MeV and the equivalent extrapolation boundary condition at $E_k = 5.0$ MeV. The initial condition is specified as (Albert & Young, 2005)

$$f = \frac{1}{p^2}\exp\left(-\frac{E_k - E_0}{\Delta E}\right)\sin\alpha, \tag{31}$$

with $E_0 = 0.2$ MeV and $\Delta E = 0.1$ MeV.

In line with the previous study (Albert & Young, 2005), our numerical tests are conducted at $L = 4.5$ for whistler-mode chorus waves (Horne, Thorne, Glauert, et al., 2005). As shown in Figure 3, the diffusion rates used here are generally consistent with those in previous works (Albert & Young, 2005; Peng et al., 2024; Tao et al., 2008, 2016). The following presents the numerical tests with uniform grids along both the α and ξ directions for the two types of precipitation loss treatments mentioned above.

Figures 4 and 5 show the electron fluxes $j = p^2 f$ at $t = 0$ and 1.0 days from the numerical tests using the boundary condition $\partial f/\partial\alpha = 0$ at $\alpha = 0°$. These tests enable us to compare the SILL and HFD schemes in terms of time step dependency, grid size dependency, and their ability to preserve positivity. Because both SILL and HFD are essentially implicit schemes, their time steps are not strictly bounded by the Courant–Friedrichs–Lewy condition. For the SILL scheme with this particular set of diffusion coefficients, the upper limit of the time step, which is inversely related to the number of grid points, is around tens of seconds. Numerical dissipation is positively correlated with the time step. With 90×80 grids, increasing the time step Δt from 1 to 20 s results in no observable variations in the electron fluxes (Figures 5a and 5c), indicating that the numerical dissipation induced by the SILL scheme is negligible compared to the physical diffusion. Reducing the number of grid points leads to a limited underestimation of the electron fluxes. In practical applications, it is necessary to balance the improvement in computational efficiency by reducing grid points with the minimization of calculation errors. In contrast to the SILL scheme, the HFD scheme cannot maintain the positivity of numerical results. However, as demonstrated in the previous work (Camporeale et al., 2013b), the nonphysical negative fluxes occur in a quite limited region inside the loss cone or near the high-energy end, where the actual fluxes are at a relatively low level. In the remaining region, the HFD scheme gives generally consistent results with the SILL scheme.

Figure 6a shows the electron flux ratio j_{HFD}/j_{SILL} at $t = 1.0$ day between the HFD and SILL schemes with 90×80 grids and a $\Delta t = 1$ s time step. Near the loss cone and above 2.0 MeV, this ratio can reach 2 or higher. Compared to HFD, which involves finite differences in f, SILL, which involves finite differences in $\ln f$, is more capable of accurately capturing the steep variations in f. When the loss term $-f/\tau_L$ is removed (Figure 6b), the sharp variations of f near the loss cone boundary disappear, and due to more significant acceleration, the energy dependence of f becomes smoother. Consequently, the results from the HFD scheme become closer to those from the SILL scheme. When only the loss term $-f/\tau_L$ is included and other diffusion terms are excluded (Figure 6c), relative to the exact solution

$$j = j|_{t=0}\exp\left(-\frac{t}{\tau_L}\right), \tag{32}$$

the SILL scheme provides accurate results, while the HFD scheme yields results with continuously accumulating errors. These results once again demonstrate that the SILL scheme surpasses the HFD scheme in terms of accuracy.

Figure 7 shows the results from the SILL scheme with the fixed precipitation boundary condition $f|_{\alpha=\alpha_L} = 0$, in comparison to those with the equivalent extrapolation precipitation boundary condition. Note that the boundary condition $f|_{\alpha=\alpha_L} = 0$ is implemented similarly to the method described in Equations 24 and 27.

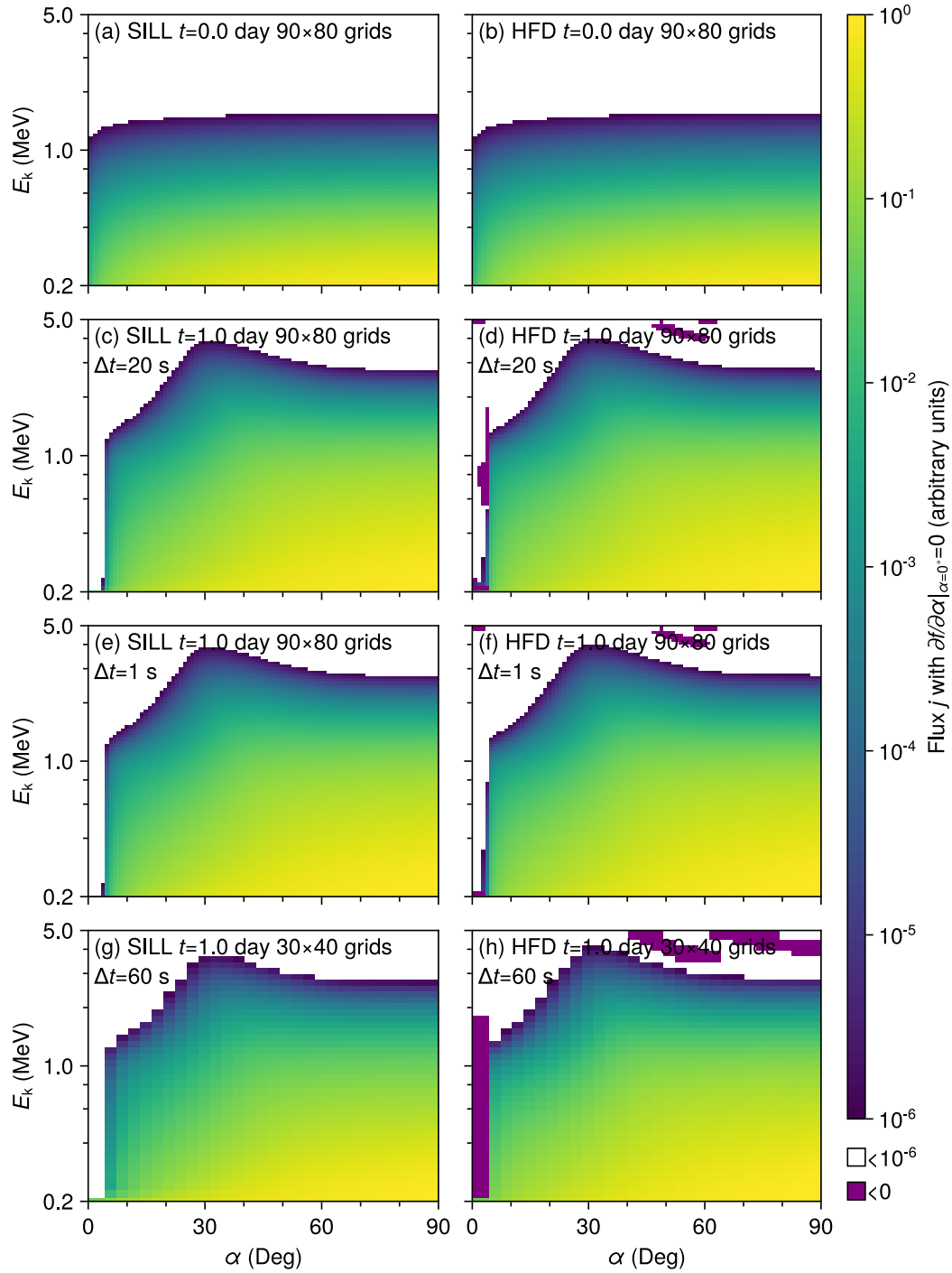

Figure 4. Numerical solutions of the chorus-driven diffusion problem with the equivalent extrapolation precipitation boundary condition. The left and right columns show the electron fluxes from the Semi-Implicit Logarithmic Linearization and Hybrid Finite Difference schemes, respectively. The first row shows the initial electron fluxes, and the other rows show the electron fluxes at $t = 1.0$ day with the indicated time steps and grids.

Because the pitch-angle diffusion rates near the loss cone are quite weak, the two types of boundary conditions essentially lead to the same results. However, because of the shift in the left pitch-angle boundary from 0° to α_L and the absence of sharp changes in f from the inside to the outside of the loss cone, the allowed time step of the SILL scheme can reach several hundreds of seconds. With 85 × 80 grids, increasing the time step Δt

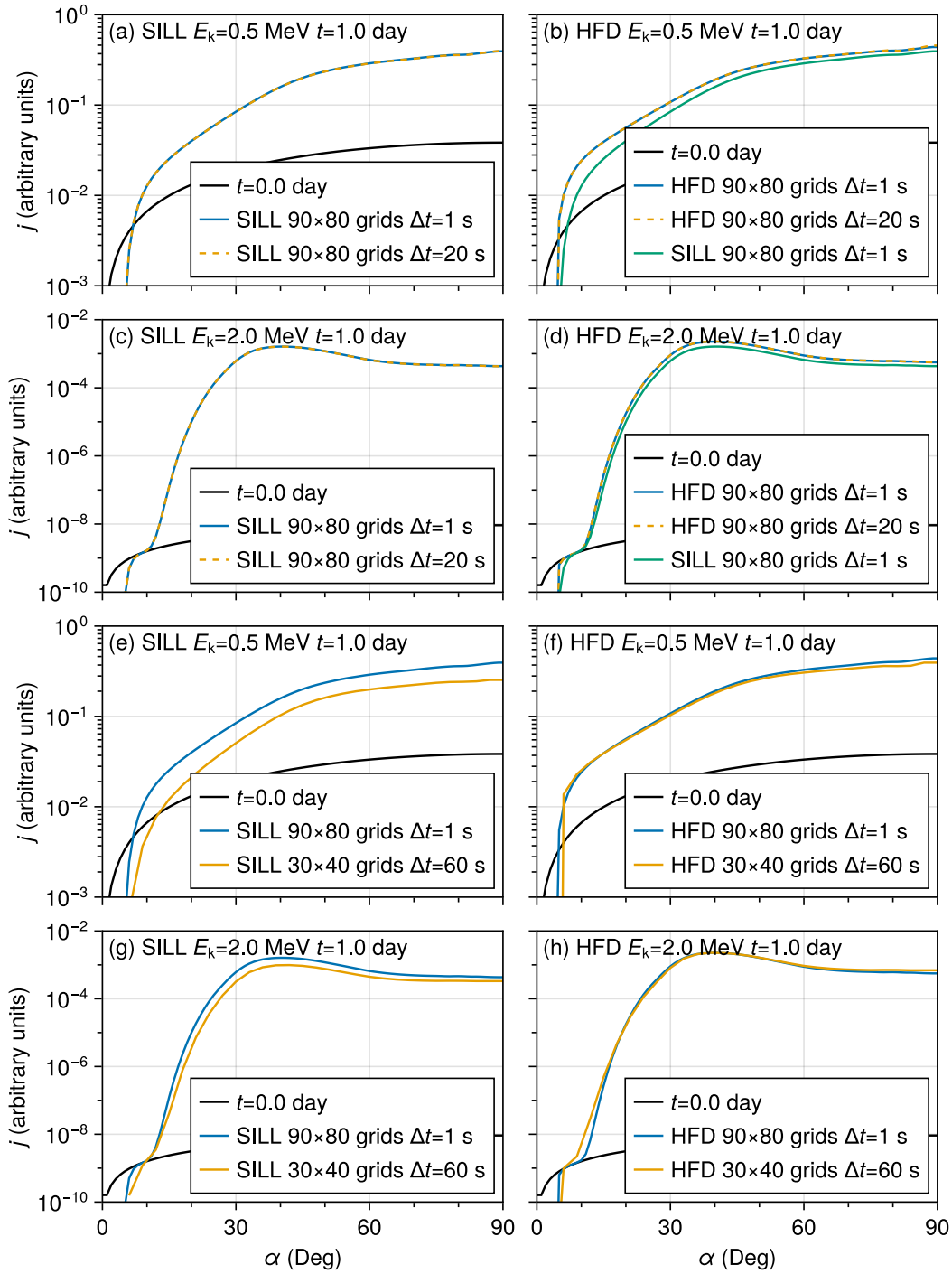

Figure 5. Comparison among the electron flux profiles at $t = 1.0$ day from simulations with the same equivalent extrapolation precipitation boundary condition but with different numerical schemes, grids, or time steps.

from 1 to 150 s results in no observable variations in the electron fluxes, reinforcing the conclusion that numerical dissipation is negligible compared to physical diffusion. Further reducing the number of grid points to 28 × 40 and increasing the time step to 300 s causes a limited underestimation of the electron fluxes, indicating once again the necessity to balance the improvement in computational efficiency by reducing grid points with the minimization of calculation errors.

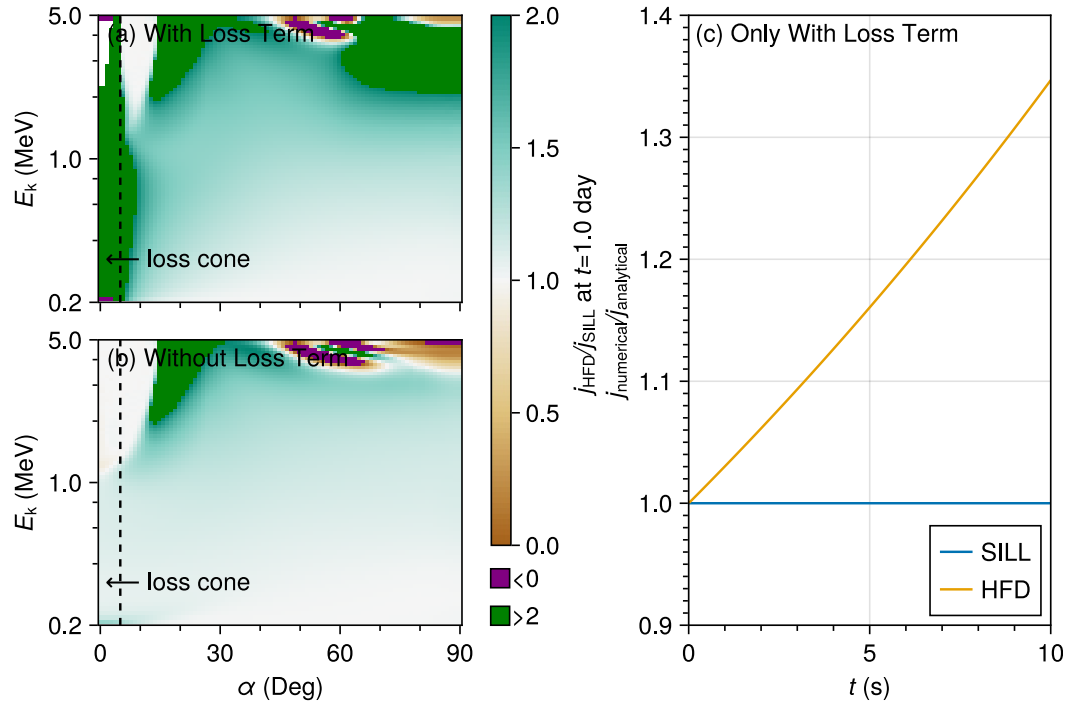

Figure 6. Comparison of accuracy between the Semi-Implicit Logarithmic Linearization (SILL) and Hybrid Finite Difference (HFD) schemes. (a) Electron flux ratio between the HFD and SILL solutions of the chorus-driven diffusion problem with the loss term. (b) Electron flux ratio between the HFD and SILL solutions of the chorus-driven diffusion problem without the loss term. (c) Electron flux ratio between the numerical and analytical solutions to the equation with only the loss term. The blue and yellow lines represent the results from the SILL and HFD schemes, respectively.

3.4. Two-Dimensional Diffusion Tests Under Extreme Conditions

We continue to focus on Equation 28, with the diffusion rates shown in Figure 3. We modify the initial condition as follows

$$f = \frac{1}{p^2}\exp\left(-\left(\frac{E_k - E_0}{\Delta E}\right)^2\right)\sin\alpha + f_0, \tag{33}$$

where $E_0 = 1.0$ MeV, $\Delta E = 0.1$ MeV, and f_0 is a free parameter controlling the orders of magnitude spanned by the PSD. All four boundary conditions are modified to equivalent extrapolation conditions.

When $f_0 = 10^{-300}$, the intial PSD decreases approximately 300 orders of magnitude from 1 to 5 MeV. As shown in Figure 8, while the HFD scheme produces a series of negative stripes, the SILL scheme preserves the positivity of the solution. However, the ability of the SILL scheme to capture extremely subtle changes in PSD comes at the cost of requiring a reduced time step to $\Delta t = 1.0$ s. If one does not care about such subtle variations in PSDs, the oversensitivity limitation of the SILL scheme may be partially avoided by increasing f_0. For example, when $f_0 = 10^{-14}$, the allowed time step for the SILL scheme increases to $\Delta t = 10$ s. Meanwhile, the increase of f_0 results in a significant reduction of the domain where negative values occur in the HFD solution.

4. Summary

We have proposed an efficient positivity-preserving finite difference scheme, SILL, for solving the Fokker-Planck diffusion equation. The expected positivity of the PSD is achieved by solving the equation of the natural logarithmic PSD. An additional advantage of logarithmization is the high accuracy in capturing the steep spatial variations in PSD, while an additional disadvantage is the introduction of nonlinearity. This multi-dimensional nonlinear problem is decomposed into one-dimensional sub-problems. Each sub-problem is

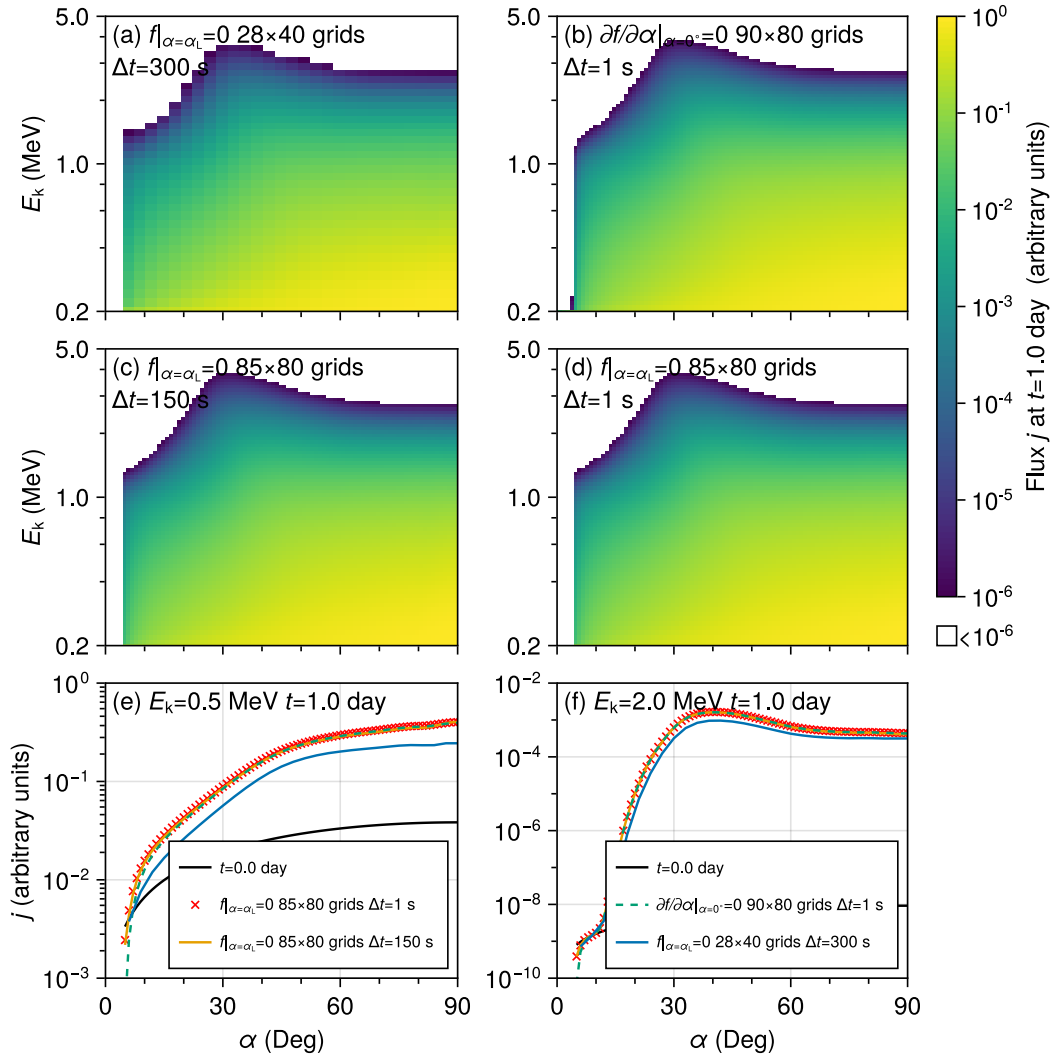

Figure 7. Numerical solutions of the chorus-driven diffusion problem using the Semi-Implicit Logarithmic Linearization scheme with different boundary conditions, grids or time steps.

solved using a semi-implicit finite difference method, where the partial derivatives multiplied by factors depending on the diagonal diffusion coefficients are treated implicitly, while the partial derivatives multiplied by factors depending on the cross diffusion coefficients are treated explicitly. The inherent nonlinearity is eliminated by replacing the traditional arithmetic mean with the geometric mean. At each time step, the SILL scheme involves solving tridiagonal systems of linear equations, which are computationally inexpensive, and the number of such systems solved is equal to the dimension of the problem, which is half that for the non-positivity-preserving HFD scheme (Xiao et al., 2009). Because of the implicit nature of the SILL scheme, its time step is not limited by the Courant–Friedrichs–Lewy condition. In general, this scheme balances positivity-preservation, ease of implementation, efficiency, and accuracy, which may be useful for the radiation belt modeling community. For the typical chorus wave-driven diffusion of radiation belt electrons, the time step can reach hundreds of seconds, which is approximately one order of magnitude higher than that for the positivity-preserving finite volume method (Gao & Wu, 2015; Peng et al., 2024) but one order of magnitude lower than that for the non-positivity-preserving FI finite difference method (D. Subbotin et al., 2010). Our computational model (Su, 2025) can simulate the two-dimensional evolution of the radiation belt electrons over a full day in several seconds. Nonetheless, like any numerical scheme, the SILL scheme has its limitations. While it is highly effective at capturing extremely subtle changes in PSDs, this same sensitivity can become a drawback when dealing with

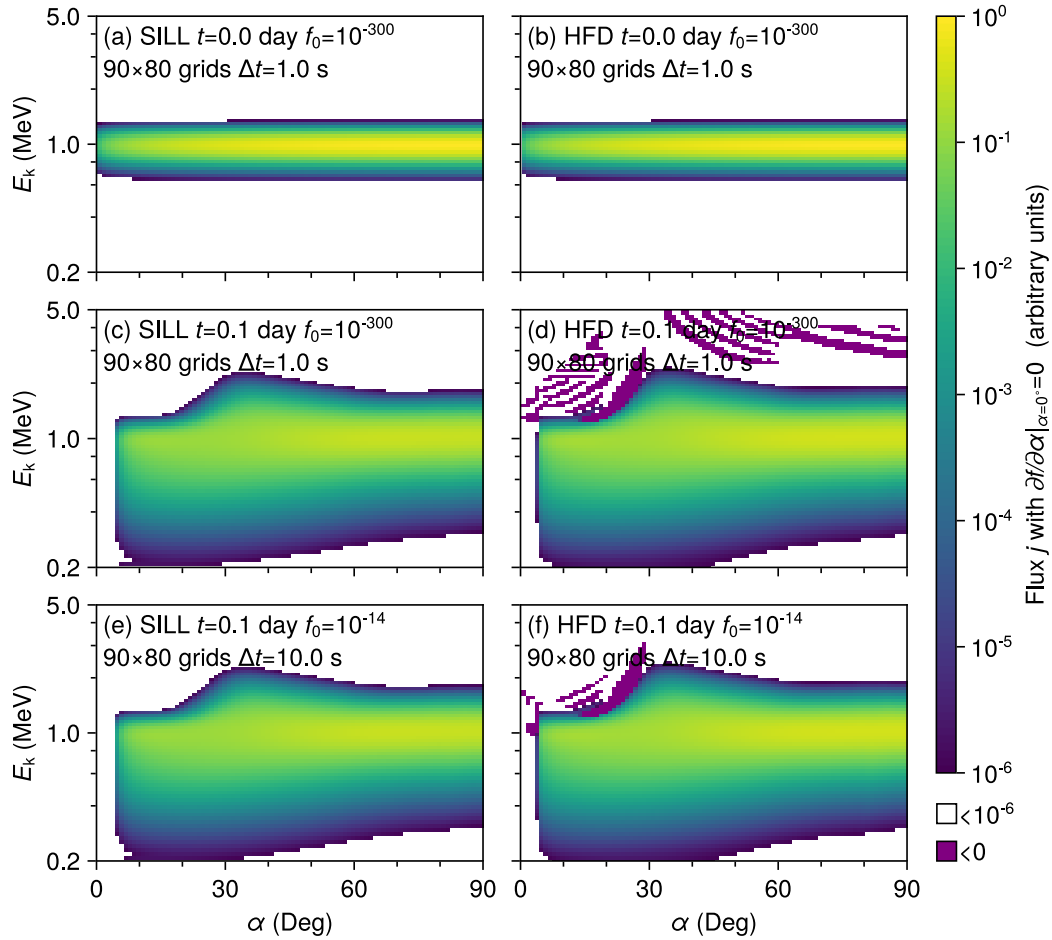

Figure 8. Comparison between numerical solutions from the Semi-Implicit Logarithmic Linearization (left) and Hybrid Finite Difference (right) schemes (a), (b) Initial phase space density distribution with $f_0 = 10^{-300}$. (c), (d) Numerical solutions at $t = 0.1$ day with $f_0 = 10^{-300}$ and $\Delta t = 1$ s. (e), (f) Numerical solutions at $t = 0.1$ day with $f_0 = 10^{-14}$ and $\Delta t = 10$ s.

near-vanishing PSDs. Particularly when the PSD exhibits extremely large variations in orders of magnitude between neighboring grid points, the performance of the SILL scheme may be compromised, necessitating a sufficiently small time step to maintain numerical stability.

Data Availability Statement

A protype Julia code of the SILL scheme is available at Su (2025).

Acknowledgments
This work was supported by the National Natural Science Foundation of China Grants 42188101, 42441808, 42130204, and 42274198, the Postdoctoral Fellowship Program of China Postdoctoral Science Foundation GZB20240701 and the open project fund of State Key Laboratory of Lunar and Planetary Sciences 002/2024/SKL.

References

Albert, J. M. (2004). Using quasi-linear diffusion to model acceleration and loss from wave-particle interactions. *Space Weather*, *2*(9), S09S03. https://doi.org/10.1029/2004SW000069

Albert, J. M. (2013). Comment on "On the numerical simulation of particle dynamics in the radiation belt. Part I: Implicit and semi-implicit schemes" and "On the numerical simulation of particle dynamics in the radiation belt. Part II: Procedure based on the diagonalization of the diffusion tensor" by E. Camporeale et al. *Journal of Geophysical Research (Space Physics)*, *118*(12), 7762–7764. https://doi.org/10.1002/2013JA019126

Albert, J. M. (2018). Diagonalization of diffusion equations in two and three dimensions. *Journal of Atmospheric and Solar-Terrestrial Physics*, *177*, 202–207. https://doi.org/10.1016/j.jastp.2017.08.008

Albert, J. M., Meredith, N. P., & Horne, R. B. (2009). Three-dimensional diffusion simulation of outer radiation belt electrons during the 9 October 1990 magnetic storm. *Journal of Geophysical Research (Space Physics)*, *114*(A9), A09214. https://doi.org/10.1029/2009JA014336

Albert, J. M., & Young, S. L. (2005). Multidimensional quasi-linear diffusion of radiation belt electrons. *Geophysical Research Letters*, *32*(14), L14110. https://doi.org/10.1029/2005GL023191

Baker, D. N., Kanekal, S. G., Li, X., Monk, S. P., Goldstein, J., & Burch, J. L. (2004). An extreme distortion of the Van Allen belt arising from the "Hallowe'en" solar storm in 2003. *Nature*, *432*(7019), 878–881. https://doi.org/10.1038/nature03116

Beutier, T., & Boscher, D. (1995). A three-dimensional analysis of the electron radiation belt by the salammbô code. *Journal of Geophysical Research (Space Physics)*, *100*(A8), 14853–14862. https://doi.org/10.1029/94JA03066

Blake, J. B., Kolasinski, W. A., Fillius, R. W., & Mullen, E. G. (1992). Injection of electrons and protons with energies of tens of MeV into L less than 3 on 24 March 1991. *Geophysical Research Letters*, *19*(8), 821–824. https://doi.org/10.1029/92GL00624

Bortnik, J., & Thorne, R. M. (2010). Transit time scattering of energetic electrons due to equatorially confined magnetosonic waves. *Journal of Geophysical Research (Space Physics)*, *115*(A7), A07213. https://doi.org/10.1029/2010JA015283

Camporeale, E., Delzanno, G. L., Zaharia, S., & Koller, J. (2013a). On the numerical simulation of particle dynamics in the radiation belt: 1. Implicit and semi-implicit schemes. *Journal of Geophysical Research (Space Physics)*, *118*(6), 3463–3475. https://doi.org/10.1002/jgra.50293

Camporeale, E., Delzanno, G. L., Zaharia, S., & Koller, J. (2013b). On the numerical simulation of particle dynamics in the radiation belt: 2. Procedure based on the diagonalization of the diffusion tensor. *Journal of Geophysical Research (Space Physics)*, *118*(6), 3476–3484. https://doi.org/10.1002/jgra.50278

Camporeale, E., Delzanno, G. L., Zaharia, S., & Koller, J. (2013c). Reply to comment by J. M. Albert on "On the numerical simulation of particle dynamics in the radiation belt. Part I: Implicit and semi-implicit schemes" and "On the numerical simulation of particle dynamics in the radiation belt. Part II: Procedure based on the diagonalization of the diffusion tensor". *Journal of Geophysical Research (Space Physics)*, *118*(12), 7765–7767. https://doi.org/10.1002/2013JA019389

Evans, D. J., & Sanugi, B. B. (1987). A comparison of numerical o.d.e. solvers based on arithmetic and geometric means. *International Journal of Computer Mathematics*, *23*(1), 37–62. https://doi.org/10.1080/00207168708803607

Fok, M.-C., Horne, R. B., Meredith, N. P., & Glauert, S. A. (2008). Radiation Belt Environment model: Application to space weather nowcasting. *Journal of Geophysical Research (Space Physics)*, *113*(A12), A03S08. https://doi.org/10.1029/2007JA012558

Fu, S., Ni, B., Zhou, R., Cao, X., & Gu, X. (2019). Combined scattering of radiation belt electrons caused by landau and bounce resonant interactions with magnetosonic waves. *Geophysical Research Letters*, *46*(10313), 10313–10321. https://doi.org/10.1029/2019GL084438

Gao, Z., & Wu, J. (2015). A second-order positivity-preserving finite volume scheme for diffusion equations on general meshes. *SIAM Journal on Scientific Computing*, *37*(1), A420–A438. https://doi.org/10.1137/140972470

Glauert, S. A., Horne, R. B., & Meredith, N. P. (2014). Three-dimensional electron radiation belt simulations using the BAS Radiation Belt Model with new diffusion models for chorus, plasmaspheric hiss, and lightning-generated whistlers. *Journal of Geophysical Research (Space Physics)*, *119*(1), 268–289. https://doi.org/10.1002/2013JA019281

Gourlay, A., & McKee, S. (1977). The construction of hopscotch methods for parabolic and elliptic equations in two space dimensions with a mixed derivative. *Journal of Computational and Applied Mathematics*, *3*(3), 201–206. https://doi.org/10.1016/S0377-0427(77)80009-5

He, Z., Yan, Q., Chu, Y., & Cao, Y. (2016). Wave-driven gradual loss of energetic electrons in the slot region. *Journal of Geophysical Research (Space Physics)*, *121*(9), 8614–8623. https://doi.org/10.1002/2016JA023087

Horne, R. B., Glauert, S. A., Meredith, N. P., Boscher, D., Maget, V., Heynderickx, D., & Pitchford, D. (2013). Space weather impacts on satellites and forecasting the Earth's electron radiation belts with SPACECAST. *Space Weather*, *11*(4), 169–186. https://doi.org/10.1002/swe.20023

Horne, R. B., & Thorne, R. M. (1998). Potential waves for relativistic electron scattering and stochastic acceleration during magnetic storms. *Geophysical Research Letters*, *25*(15), 3011–3014. https://doi.org/10.1029/98GL01002

Horne, R. B., Thorne, R. M., Glauert, S. A., Albert, J. M., Meredith, N. P., & Anderson, R. R. (2005). Timescale for radiation belt electron acceleration by whistler mode chorus waves. *Journal of Geophysical Research (Space Physics)*, *110*(A3), A03225. https://doi.org/10.1029/2004JA010811

Horne, R. B., Thorne, R. M., Shprits, Y. Y., Meredith, N. P., Glauert, S. A., Smith, A. J., et al. (2005). Wave acceleration of electrons in the Van Allen radiation belts. *Nature*, *437*(7056), 227–230. https://doi.org/10.1038/nature03939

Kim, J., Ryu, D., Jones, T. W., & Hong, S. S. (1999). A multidimensional code for isothermal magnetohydrodynamic flows in astrophysics. *The Astrophysical Journal*, *514*(1), 506–519. https://doi.org/10.1086/306915

Li, J., Ni, B., Xie, L., Pu, Z., Bortnik, J., Thorne, R. M., et al. (2014). Interactions between magnetosonic waves and radiation belt electrons: Comparisons of quasi-linear calculations with test particle simulations. *Geophysical Research Letters*, *41*(14), 4828–4834. https://doi.org/10.1002/2014GL060461

Li, L. Y., Yu, J., Cao, J. B., Yang, J. Y., Li, X., Baker, D. N., et al. (2017). Roles of whistler mode waves and magnetosonic waves in changing the outer radiation belt and the slot region. *Journal of Geophysical Research (Space Physics)*, *122*(5), 5431–5448. https://doi.org/10.1002/2016JA023634

Li, W., & Hudson, M. K. (2019). Earth's van allen radiation belts: From discovery to the van allen Probes Era. *Journal of Geophysical Research (Space Physics)*, *124*(11), 8319–8351. https://doi.org/10.1029/2018JA025940

Li, W., Shprits, Y. Y., & Thorne, R. M. (2007). Dynamic evolution of energetic outer zone electrons due to wave-particle interactions during storms. *Journal of Geophysical Research (Space Physics)*, *112*(A10), A10220. https://doi.org/10.1029/2007JA012368

Li, X., Baker, D. N., Kanekal, S. G., Looper, M., & Temerin, M. (2001). Long term measurements of radiation belts by SAMPEX and their variations. *Geophysical Research Letters*, *28*(20), 3827–3830. https://doi.org/10.1029/2001GL013586

Lyons, L. R., & Williams, D. J. (1984). *Quantitative aspects of magnetospheric physics*. Springer.

Miyoshi, Y. S., Jordanova, V. K., Morioka, A., & Evans, D. S. (2004). Solar cycle variations of the electron radiation belts: Observations and radial diffusion simulation. *Space Weather*, *2*(10), S10S02. https://doi.org/10.1029/2004SW000070

Ni, B., Huang, H., Zhang, W., Gu, X., Zhao, H., Li, X., et al. (2019). Parametric sensitivity of the formation of reversed electron energy spectrum caused by Plasmaspheric Hiss. *Geophysical Research Letters*, *46*(8), 4134–4143. https://doi.org/10.1029/2019GL082032

Peng, P., Tao, X., Peng, Z., Jiang, Y., Gao, Z., Yang, D., et al. (2024). Modeling radiation belt dynamics using a positivity-preserving finite volume method on general meshes. *Journal of Geophysical Research (Space Physics)*, *129*(9), e2024JA032919. https://doi.org/10.1029/2024JA032919

Pham, K. H., Tu, W., & Xiang, Z. (2017). Quantifying the precipitation loss of radiation belt electrons during a rapid dropout event. *Journal of Geophysical Research (Space Physics)*, *122*(10), 10287–10303. https://doi.org/10.1002/2017JA024519

Reeves, G. D., McAdams, K. L., Friedel, R. H. W., & O'Brien, T. P. (2003). Acceleration and loss of relativistic electrons during geomagnetic storms. *Geophysical Research Letters*, *30*(10), 1529. https://doi.org/10.1029/2002GL016513

Reeves, G. D., Spence, H. E., Henderson, M. G., Morley, S. K., Friedel, R. H. W., Funsten, H. O., et al. (2013). Electron acceleration in the heart of the van allen radiation belts. *Science*, *341*(6149), 991–994. https://doi.org/10.1126/science.1237743

Richtmyer, R. D., & Morton, K. W. (1967). Difference methods for initial-value problems.

Ripoll, J. F., Claudepierre, S. G., Ukhorskiy, A. Y., Colpitts, C., Li, X., Fennell, J. F., & Crabtree, C. (2020). Particle dynamics in the Earth's radiation belts: Review of current research and open questions. *Journal of Geophysical Research (Space Physics)*, *125*(5), e26735. https://doi.org/10.1029/2019JA026735

Schulz, M., & Lanzerotti, L. J. (1974). Particle diffusion in the radiation belts. In *Physics and chemistry in space* (Vol. 7, pp. 46–80). Springer-Verlag.

Selesnick, R. S., Blake, J. B., & Mewaldt, R. A. (2003). Atmospheric losses of radiation belt electrons. *Journal of Geophysical Research (Space Physics)*, *108*(A12), 1468. https://doi.org/10.1029/2003JA010160

Shprits, Y. Y. (2009). Potential waves for pitch-angle scattering of near-equatorially mirroring energetic electrons due to the violation of the second adiabatic invariant. *Geophysical Research Letters*, *36*(12), L12106. https://doi.org/10.1029/2009GL038322

Shprits, Y. Y., Chen, L., Ukhorskiy, A., & Thorne, R. (2009). Simulations of pitch-angle scattering of relativistic electrons with mlt-dependent diffusion coefficients. *Journal of Geophysical Research (Space Physics)*, *114*(A3), A03219. https://doi.org/10.1029/2008JA013695

Shprits, Y. Y., Subbotin, D., Drozdov, A., Usanova, M. E., Kellerman, A., Orlova, K., et al. (2013). Unusual stable trapping of the ultrarelativistic electrons in the van allen radiation belts. *Nature Physics*, *9*(11), 699–703. https://doi.org/10.1038/nphys2760

Strang, G. (1968). On the construction and comparison of difference schemes. *SIAM Journal on Numerical Analysis*, *5*(3), 506–517. https://doi.org/10.1137/0705041

Su, Z. (2025). ZhenpengSu/SILL: Semi-Implicit Logarithmic Linearization (SILL) scheme v0.1.1 [Software]. *Zenodo*. https://doi.org/10.5281/zenodo.14977761

Su, Z., Xiao, F., Zheng, H., & Wang, S. (2010). STEERB: A three-dimensional code for storm-time evolution of electron radiation belt. *Journal of Geophysical Research (Space Physics)*, *115*(A9), A09208. https://doi.org/10.1029/2009JA015210

Su, Z., Xiao, F., Zheng, H., & Wang, S. (2011a). CRRES observation and STEERB simulation of the 9 October 1990 electron radiation belt dropout event. *Geophysical Research Letters*, *38*(A9), L06106. https://doi.org/10.1029/2011GL046873

Su, Z., Xiao, F., Zheng, H., & Wang, S. (2011b). Radiation belt electron dynamics driven by adiabatic transport, radial diffusion, and wave-particle interactions. *Journal of Geophysical Research (Space Physics)*, *116*(A4), A04205. https://doi.org/10.1029/2010JA016228

Su, Z., Zheng, H., & Wang, S. (2010). Three dimensional simulations of energetic outer zone electron dynamics due to wave-particle interaction and azimuthal advection. *Journal of Geophysical Research (Space Physics)*, *115*(A6), A06203. https://doi.org/10.1029/2009JA014980

Subbotin, D., Shprits, Y., & Ni, B. (2010). Three-dimensional VERB radiation belt simulations including mixed diffusion. *Journal of Geophysical Research (Space Physics)*, *115*(A3), A03205. https://doi.org/10.1029/2009JA015070

Subbotin, D. A., & Shprits, Y. Y. (2009). Three-dimensional modeling of the radiation belts using the versatile electron radiation belt (VERB) code. *Space Weather*, *7*(10), S10001. https://doi.org/10.1029/2008SW000452

Subbotin, D. A., & Shprits, Y. Y. (2012). Three-dimensional radiation belt simulations in terms of adiabatic invariants using a single numerical grid. *Journal of Geophysical Research (Space Physics)*, *117*(A5), A05205. https://doi.org/10.1029/2011JA017467

Summers, D., Ni, B., & Meredith, N. P. (2007a). Timescales for radiation belt electron acceleration and loss due to resonant wave-particle interactions: 1. Theory. *Journal of Geophysical Research (Space Physics)*, *112*(A4), A04206. https://doi.org/10.1029/2006JA011801

Summers, D., Ni, B., & Meredith, N. P. (2007b). Timescales for radiation belt electron acceleration and loss due to resonant wave-particle interactions: 2. Evaluation for VLF chorus, ELF hiss, and electromagnetic ion cyclotron waves. *Journal of Geophysical Research (Space Physics)*, *112*(A4), A04207. https://doi.org/10.1029/2006JA011993

Summers, D., Thorne, R. M., & Xiao, F. (1998). Relativistic theory of wave-particle resonant diffusion with application to electron acceleration in the magnetosphere. *Journal of Geophysical Research (Space Physics)*, *103*(A9), 20487–20500. https://doi.org/10.1029/98JA01740

Tao, X., Chan, A. A., Albert, J. M., & Miller, J. A. (2008). Stochastic modeling of multidimensional diffusion in the radiation belts. *Journal of Geophysical Research (Space Physics)*, *113*(A7), A07212. https://doi.org/10.1029/2007JA012985

Tao, X., Zhang, L., Wang, C., Li, X., Albert, J. M., & Chan, A. A. (2016). An efficient and positivity-preserving layer method for modeling radiation belt diffusion processes. *Journal of Geophysical Research (Space Physics)*, *121*(1), 305–320. https://doi.org/10.1002/2015JA022064

Thorne, R. M. (2010). Radiation belt dynamics: The importance of wave-particle interactions. *Geophysical Research Letters*, *37*(22), L22107. https://doi.org/10.1029/2010GL044990

Thorne, R. M., Li, W., Ni, B., Ma, Q., Bortnik, J., Chen, L., et al. (2013). Rapid local acceleration of relativistic radiation-belt electrons by magnetospheric chorus. *Nature*, *504*(7480), 411–414. https://doi.org/10.1038/nature12889

Tu, W., Cunningham, G. S., Chen, Y., Henderson, M. G., Camporeale, E., & Reeves, G. D. (2013). Modeling radiation belt electron dynamics during GEM challenge intervals with the DREAM3D diffusion model. *Journal of Geophysical Research (Space Physics)*, *118*(10), 6197–6211. https://doi.org/10.1002/jgra.50560

Tu, W., Selesnick, R., Li, X., & Looper, M. (2010). Quantification of the precipitation loss of radiation belt electrons observed by SAMPEX. *Journal of Geophysical Research (Space Physics)*, *115*(A7), A07210. https://doi.org/10.1029/2009JA014949

Varotsou, A., Boscher, D., Bourdarie, S., Horne, R. B., Meredith, N. P., Glauert, S. A., & Friedel, R. H. (2008). Three-dimensional test simulations of the outer radiation belt electron dynamics including electron-chorus resonant interactions. *Journal of Geophysical Research (Space Physics)*, *113*(A12), A12212. https://doi.org/10.1029/2007JA012862

Wang, C., Ma, Q., Tao, X., Zhang, Y., Teng, S., Albert, J. M., et al. (2017). Modeling radiation belt dynamics using a 3-D layer method code. *Journal of Geophysical Research (Space Physics)*, *122*(8), 8642–8658. https://doi.org/10.1002/2017JA024143

Wang, D., Shprits, Y. Y., Zhelavskaya, I. S., Effenberger, F., Castillo, A. M., Drozdov, A. Y., et al. (2020). The effect of plasma boundaries on the dynamic evolution of relativistic radiation belt electrons. *Journal of Geophysical Research (Space Physics)*, *125*(5), e27422. https://doi.org/10.1029/2019JA027422

Xiao, F., Su, Z., Zheng, H., & Wang, S. (2009). Modeling of outer radiation belt electrons by multidimensional diffusion process. *Journal of Geophysical Research (Space Physics)*, *114*(A3), A03201. https://doi.org/10.1029/2008JA013580

Xiao, F., Su, Z., Zheng, H., & Wang, S. (2010). Three-dimensional simulations of outer radiation belt electron dynamics including cross diffusion terms. *Journal of Geophysical Research (Space Physics)*, *115*(A5), A05216. https://doi.org/10.1029/2009JA014541

Xiao, F., Yang, C., Su, Z., Zhou, Q., He, Z., He, Y., et al. (2015). Wave-driven butterfly distribution of van allen belt relativistic electrons. *Nature Communications*, *6*(1), 8590. https://doi.org/10.1038/ncomms9590

Yu, J., Ren, A., He, Z., Liu, X., Wang, J., Liu, N., et al. (2024). Resonant interactions between relativistic electrons and EMIC waves modified by partial shell proton velocity distributions. *Journal of Geophysical Research (Space Physics)*, *129*(4), e2023JA032355. https://doi.org/10.1029/2023JA032355

Yuan, Z., Liu, K., Yu, X., Yao, F., Huang, S., Wang, D., & Ouyang, Z. (2018). Precipitation of radiation belt electrons by EMIC waves with conjugated observations of NOAA and van allen satellites. *Geophysical Research Letters*, *45*(23), 12694–12702. https://doi.org/10.1029/2018GL080481

Zhao, H., Ni, B., Li, X., Baker, D. N., Johnston, W. R., Zhang, W., et al. (2019). Plasmaspheric hiss waves generate a reversed energy spectrum of radiation belt electrons. *Nature Physics*, *15*(4), 367–372. https://doi.org/10.1038/s41567-018-0391-6

Zong, Q., Zhou, X., Wang, Y. F., Li, X., Song, P., Baker, D. N., et al. (2009). Energetic electron response to ULF waves induced by interplanetary shocks in the outer radiation belt. *Journal of Geophysical Research (Space Physics)*, *114*(A10), A10204. https://doi.org/10.1029/2009JA014393